Journal of Inclusion Phenomena and Molecular Recognition in Chemistry **8**: 71–88, 1990.

Depressurization of Natural Gas Hydrates in Berea Sandstone Cores*

M. H. YOUSIF, P. M. LI,** M. S. SELIM, and E. D. SLOAN‡
Chemical Engineering and Petroleum Refining Department, Colorado School of Mines, Golden, CO 80401, U.S.A.

(Received: 22 February 1988; in final form: 3 May 1988)

Abstract. D. W. Davidson *et al.* [7] were among the first to recognize significant deposits of natural gas clathrate hydrates in the Western Hemisphere. This work discusses the recovery of gas from such deposits, through laboratory measurement and modeling of a depressurization scheme. The work provides a determination of the volume of gas produced and the position of the hydrate interface, as a function of time when a hydrate-containing core is depressurized. A moving boundary model is shown to provide a satisfactory fit to hydrate dissociation measurements. Qualitative information is provided concerning hydrate formation in Berea Sandstone cores.

Key words. Depressurization, dissociation, gas hydrate.

1. Introduction

More than a decade ago, Davidson and coworkers [7] indicated the existence of natural gas clathrate hydrate deposits in the Canadian permafrost, following similar reports of gas hydrate deposits in the U.S.S.R. by Cherskii and Makogon [4]. Since every volume of hydrate has the potential to contain about 170 volumes of gas, the amount of gas contained in a hydrate deposit can be substantial. Makogon [12] recently estimated that the total natural gas contained in hydrates was at least two orders of magnitude greater than that in the proven gas reserves. Kvenvolden and co-workers [11] have reported evidence of hydrates at several world-wide locations, as indicated by each dot in Figure 1.

Such studies have revitalized industrial interest in these inclusion compounds, which had been previously considered only as nuisances to the gas industry. Davidson [6] summarized the molecular properties of these clathrate structures in a chapter to which every serious student of clathrates must eventually turn. Several laboratory schemes and models [2, 5, 9, 10, 14] have been suggested for the determination of gas production from hydrate reserves. However, the only known instance of production of a hydrate reserve has been the Messoyakha field in the U.S.S.R. [12], where the gas hydrate overlies the gas reserve. Production in that instance has been primarily through depressurization of the gas reservoir, so that the gas hydrate replenished the reserve, over a fifteen year period.

Laboratory workers have not been successful at quantifying hydrate formation and dissociation in consolidated sediments, as a simulation of occurrences in an

* Dedicated to Dr D. W. Davidson in honor of his great contributions to the sciences of inclusion phenomena.

** East China Petroleum Institute.
‡ Author for correspondence.

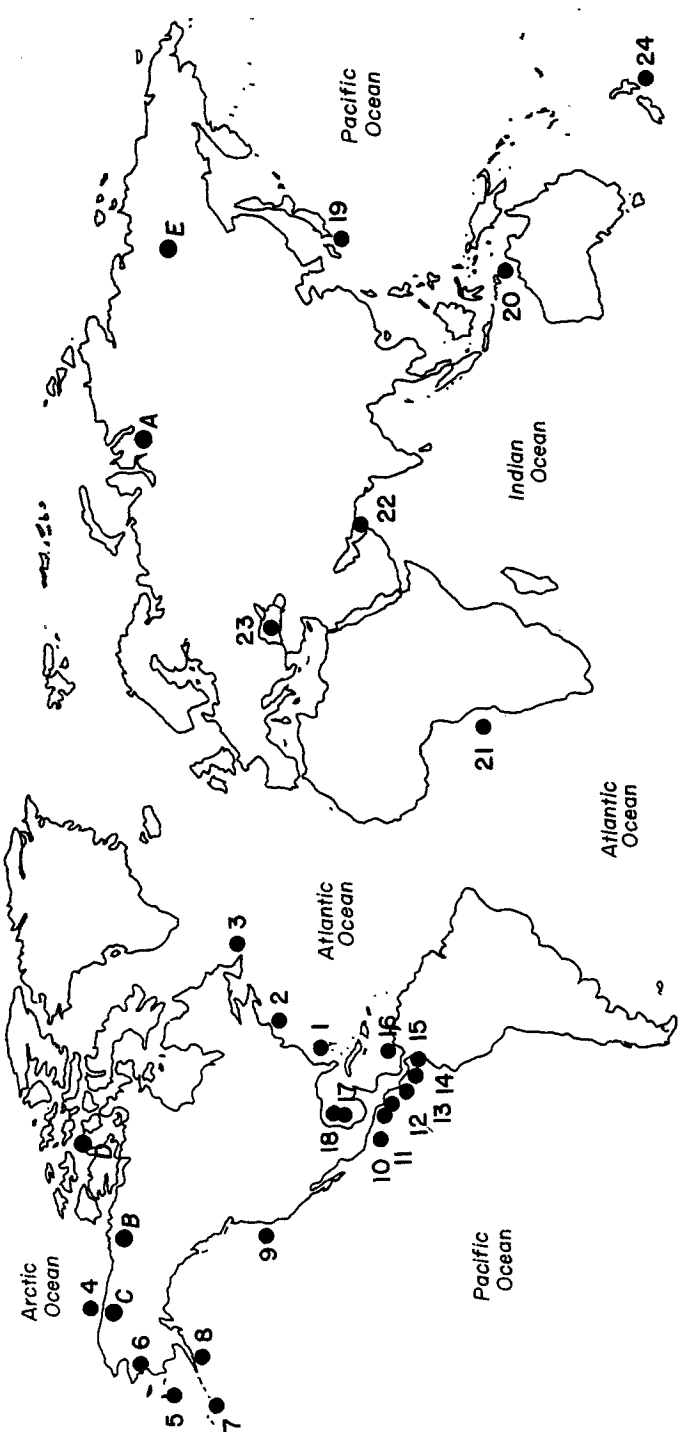

Fig. 1. Sites of world-wide evidence of natural gas hydrates.

actual hydrate reserve. Published attempts [1, 8] illustrate the difficulty of such an experimental effort.

One of the objectives of this work was to form hydrates in a Berea Sandstone core, and to measure the dissociation rate of such hydrates taking advantage of electrical resistivity measurements [16], to monitor the position of the hydrate front. The second objective of this work was to formulate an analytical model, based on first principles, with which one could approximate the hydrate dissociation process on depressurization.

2. Experimental Apparatus and Procedure

2.1. APPARATUS

A diagram of the experimental apparatus is given in Figure 2. The central part of the apparatus was a Berea Sandstone cylindrical core (0.1524 m long × 0.0381 m diameter). The core was enclosed within a heat-shrunk plastic tube and contained within a stainless steel pressure sample bomb. An external pressure, which was at least 0.35 MPa greater than that within the core, was maintained on the outside of the heat-shrink tubing with a manual hydraulic pump.

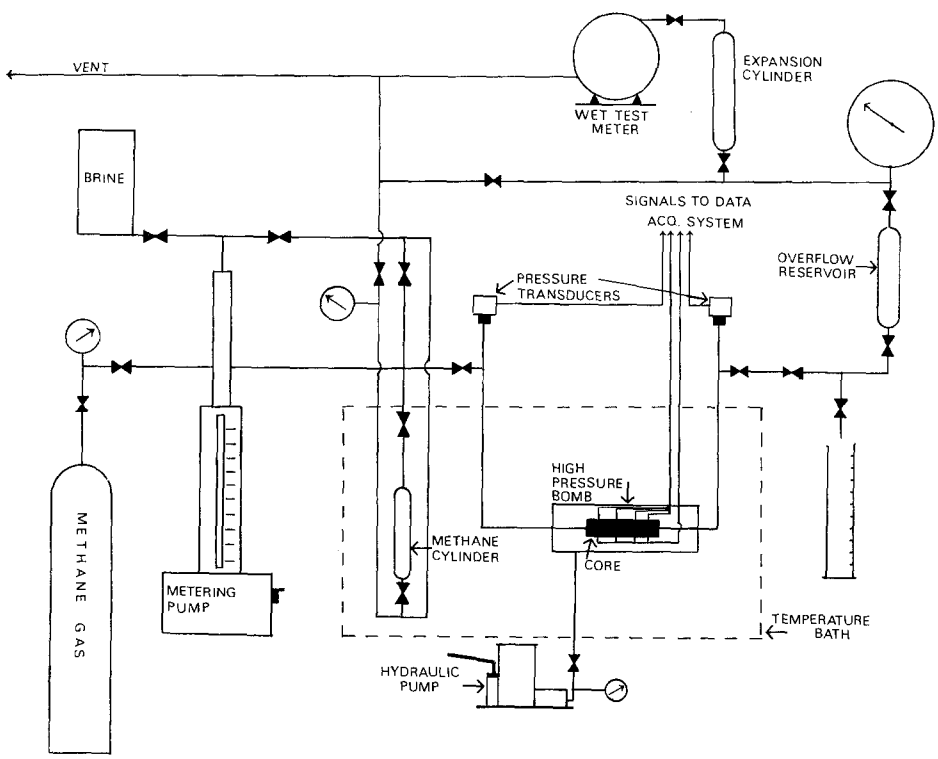

Fig. 2. Experimental apparatus.

Four pairs of electrodes were implanted at equal distances along the core length, under the heat-shrink tubing, in order to track the location of the hydrate dissociation front. A high (1000 Hz) frequency current was used, and the voltage drop was measured across four known resistors, each connected in series with the core electrodes. The resistance across each electrode was determined by the equation:

$$R_{e_i} = R_{r_i}\left(\frac{V_g}{V_{r_i}} - 1\right) \tag{1}$$

where: R_{e_i} = electrical resistance of the electrode i; R_{r_i} = reference resistor i; V_g = voltage drop across the function generator; and V_{r_i} = voltage drop across the reference resistor.

The flow system to inject both water and gas into the core, consisted of a pressure-controlled metering pump. The pump was an ISCO® model 314 syringe pump, which had a variable rate from 0.8 to 200 $\times 10^{-6}$ m^3/hr. The pressure control unit was made by Eldex, and controlled the injection rate of the pump to maintain the pressure to within ± 172 kPa of the desired setting. The injection rate of 80×10^{-6} m^3/h was normally used. Methane gas was injected from the methane cylinder indicated on the diagram by water displacement.

The temperature of the system was maintained at 273.7 K in a bath with a fluid mixture of 50 mass percent ethylene glycol–water. The bath was refrigerated by a Lauda IC-6® unit, and the final temperature was controlled by a NESLAB® Exatrol unit, accurate to within ± 0.25 K. The temperature was checked periodically using a mercury thermometer.

In addition to the resistance measurements along the core, measurements were made of inlet and outlet pressure, as well as the volumes of injected and produced fluids – all as a function of time. The two pressures were determined by 0–10 MPa Omega® transducers, which had an accuracy to within 0.5% of full range. The volume was determined by water displacement into a graduated cylinder, with readings obtained every minute.

A Keithly®-500 system was used for data acquisition, interfaced with an IBM®-XT computer. Pressures and resistances were recorded at 10 minute intervals during hydrate formation, and at 30 second intervals during hydrate dissociation.

2.2. EXPERIMENTAL PROCEDURE

Several preliminary experimental iterations were performed before the following procedure was determined. The core was initially evacuated, before being fully saturated with 1.5% (mass) sodium chloride solution at the experimental temperature and pressure. Several pore volumes of saline solution were circulated for stability and full saturation of the core.

One pore volume of methane gas was injected at the experimental temperature and pressure. Hydrates began forming and caused flow restrictions during the stage of gas injection, as indicated by the large pressure drop across the cell. During this period both the gas and water volumes injected and produced were closely monitored. The water produced was subtracted from the total pore volume to determine the water available for hydrate formation. Both the inlet and the outlet

valve of the core were then closed to allow hydrate formation to continue, typically over 24 to 30 hours. When the pressure no longer decreased with time, the hydrate formation stopped, always at pressures greater than the equilibrium three-phase pressure of 2.84 MPa.

Hydrates were dissociated at a constant temperature of 273.7 K and at constant outlet pressures of 1.47 and 2.5 MPa. The inlet pressure, the gas volume (at 294 K and 90.94 kPa), and the resistance changes along the core length were the primary variables measured with time upon hydrate dissociation. During dissociation, the effective permeability measurements were determined by means of Darcy's Law, using the pressure drop across the core and the gas production rate.

3. Experimental Results

3.1. HYDRATE FORMATION

Qualitative observations were made upon hydrate formation regarding the effect of core permeability, resistivity changes, and position of hydrate formation within the core. Via preliminary formation experiments with two cores which had permeabilities of 8.388×10^{-14} and 40×10^{-14} m^2, it was determined that, while the lower permeability core required 20–30 hours to complete the formation process, the high permeability core required only 4–5 hours for formation. In addition, the high permeability core could not be plugged with hydrate as readily as the low permeability core.

Figure 3 presents the pressure reduction results on hydrate formation for Run 1 of the low permeability core. Upon formation, a restriction frequently occurred near the inlet of the low permeability core. The figure shows that, when both valves were closed, the inlet pressure decreased below that of the outlet pressure. On repressurization with gas, the inlet pressure continued to decrease below that of the outlet. This indicated that hydrates formed rapidly at the inlet, and the gas passageway was effectively blocked, preventing the outlet pressure from equilibrating with the inlet.

Figure 4 presents the pressure curve on hydrate formation for Run 2. The outlet pressure decreased rapidly, and then automatically recovered. This behavior can be attributed to the rapid hydrate formation near the outlet, resulting in a partial plugging which subsequently was automatically removed by the large pressure gradient. During the later portions of the hydrate formation for Run 2, the slopes of both pressure curves were nearly equal, indicating good gas communication, and a more even hydrate formation throughout the core.

Figure 5 shows the pressure curve on hydrate formation for Run 3. In this run, in order to ensure more uniform hydrate distribution along the core, the hydrate was dissociated and reformed in two cycles (A1 and A2) of an annealing process. In the annealing process the hydrate is dissociated and reformed by cyclical heating and cooling of the core.

During hydrate formation for each run, the resistance measurements increased uniformly and simultaneously, and thus could not be used to determine where hydrate formation had occurred.

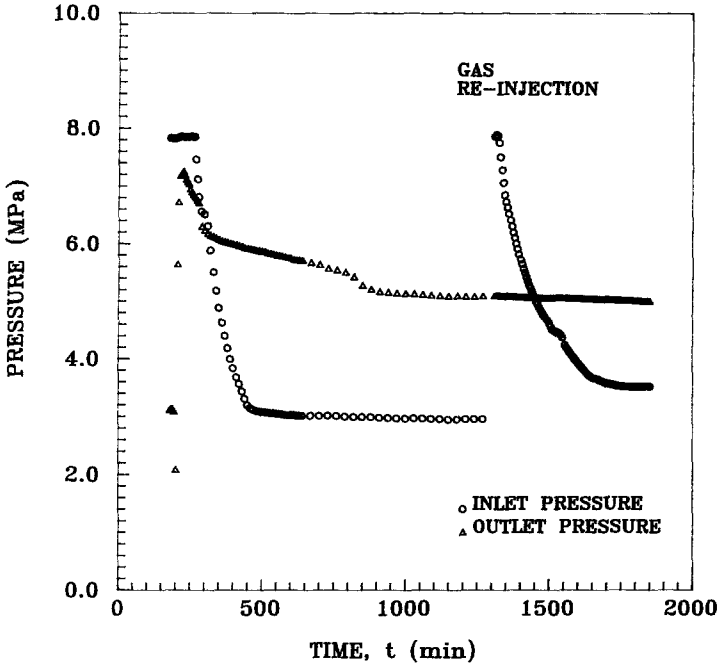

Fig. 3. Hydrate formation pressure versus time for Run 1.

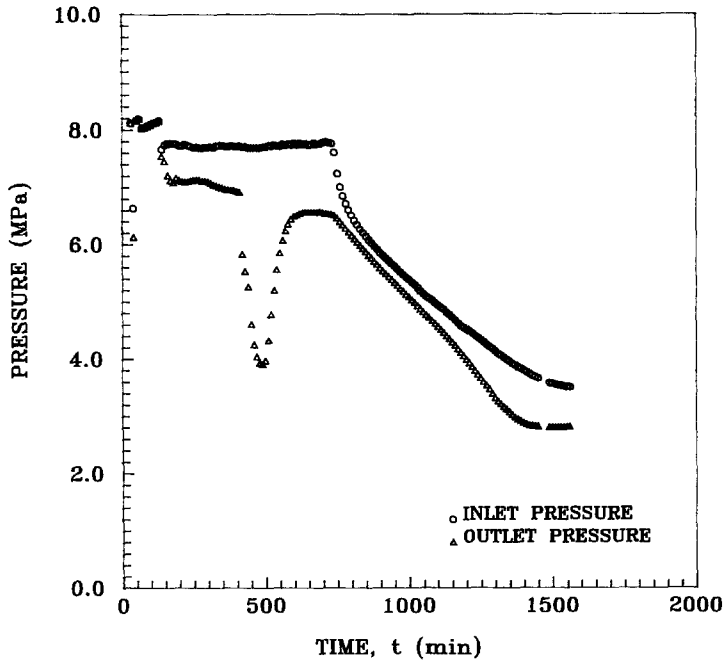

Fig. 4. Hydrate formation pressure versus time for Run 2.

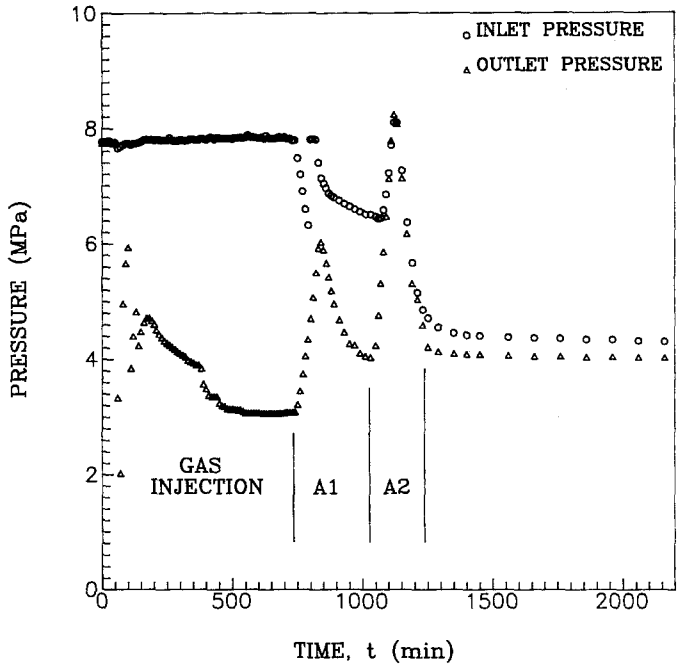

Fig. 5. Hydrate formation pressure versus time for Run 3.

3.2. HYDRATE DISSOCIATION

Figure 6 presents the pressure versus time curves for hydrate dissociation for Run 1. After the pressures were stable for some time the dissociation experiment was begun. After 18 minutes the outlet pressure was decreased to 1.47 MPa, approximately one-half that of the equilibrium pressure (2.84 MPa). Approximately five minutes later, the inlet pressure started to decrease sharply indicating that the hydrate had dissociated sufficiently to allow gas communication between both measuring points. With a constant outlet pressure, the inlet pressure slope then decreased as more hydrate dissociated, before finally increasing on hydrate depletion to join that of the discharge pressure. In the figure the missing data between 30 to 35 minutes are due to data acquisition malfunction.

Figure 7 presents the dissociation pressure curve for Run 2, in contrast to Figure 6. At approximately 20 minutes, when the outlet pressure was decreased from 3.35 MPa to 2.5 MPa, a value only slightly less than the equilibrium pressure, the inlet pressure remained relatively constant until 155 minutes. Run 3 gave a similar performance to Run 2, as presented in Figure 8. Dissociation was conducted at 2.64 MPa, below the equilibrium pressure. The inlet pressure remained constant for almost 150 minutes. This inlet pressure stability was evidence that the hydrate dissociation front did not receed to the inlet of the core for almost two hours. By reviewing Makogon's data [12], we suggest that such incremental pressure reduction below the equilibrium value may simulate hydrate production from the Messoyakha gas field. We infer from this that a moving boundary model is appropriate for such data.

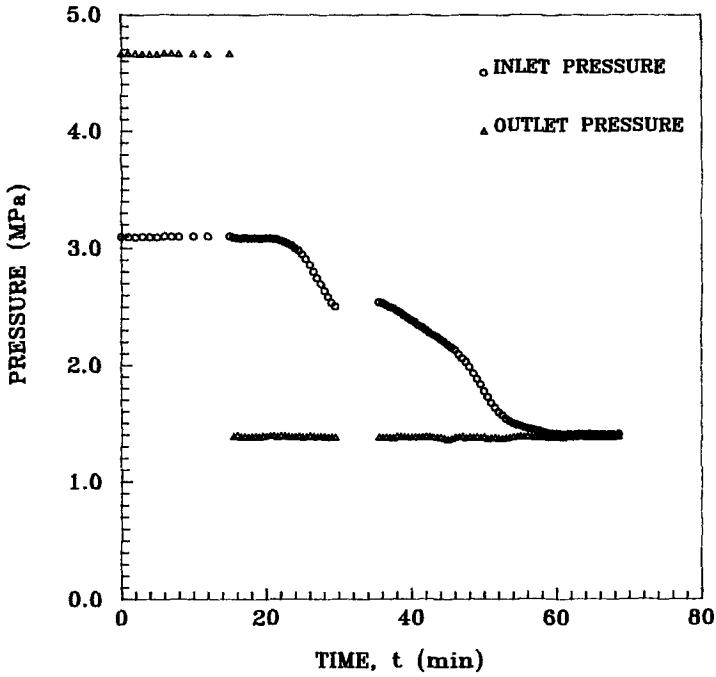

Fig. 6. Hydrate dissociation pressure versus time for Run 1.

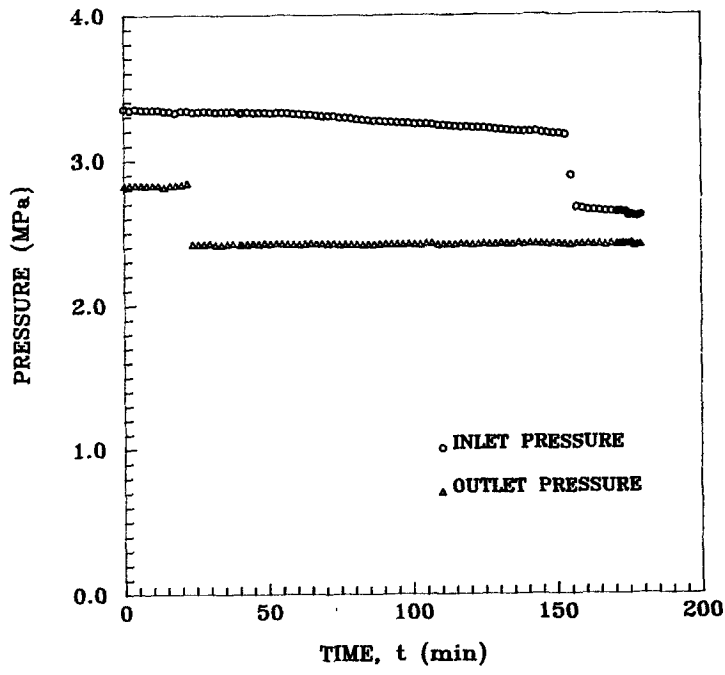

Fig. 7. Hydrate dissociation pressure versus time for Run 2.

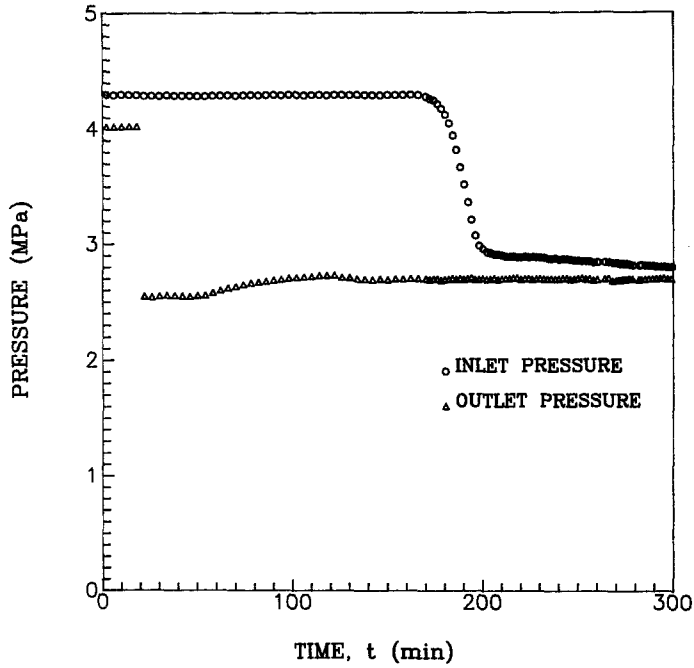

Fig. 8. Hydrate dissociation pressure versus time for Run 3.

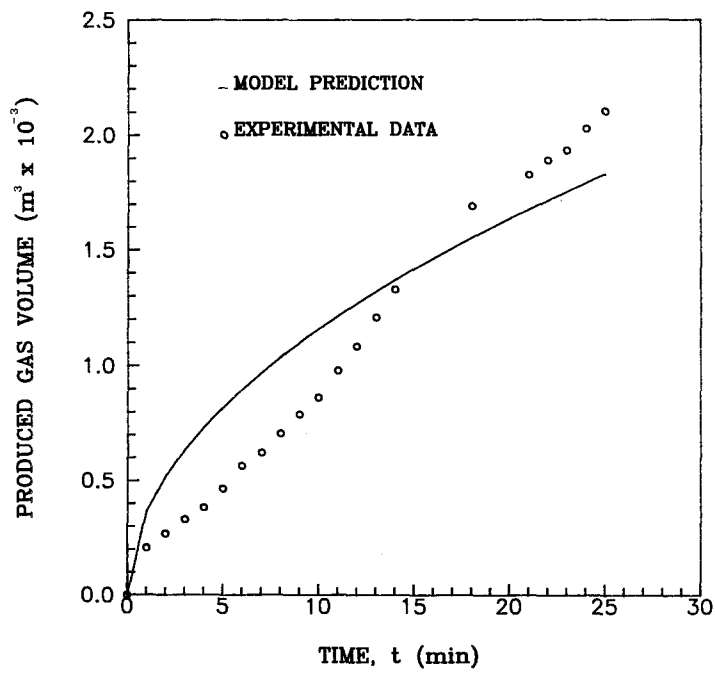

Fig. 9. Dissociated gas volume versus time for Run 1.

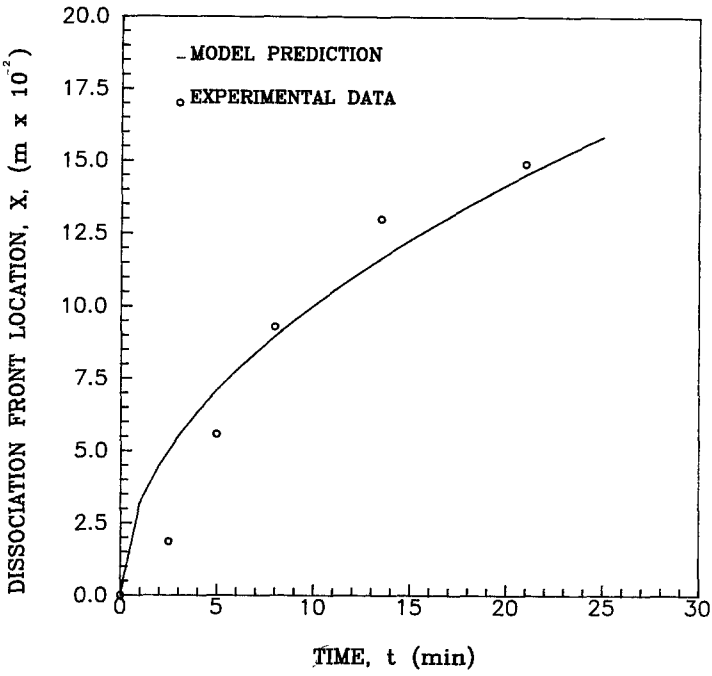

Fig. 10. Position of dissociated front versus time for Run 1.

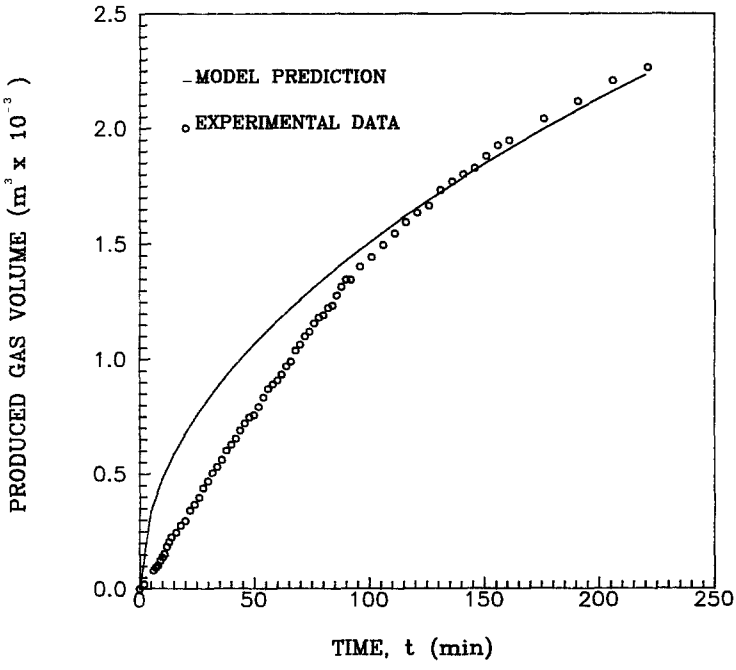

Fig. 11. Dissociated gas volume versus time for Run 2.

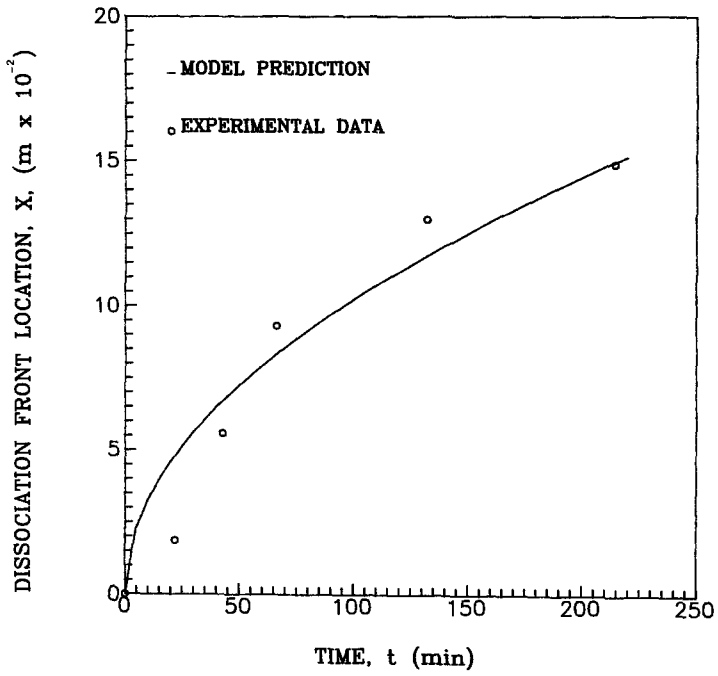

Fig. 12. Position of dissociated front versus time for Run 2.

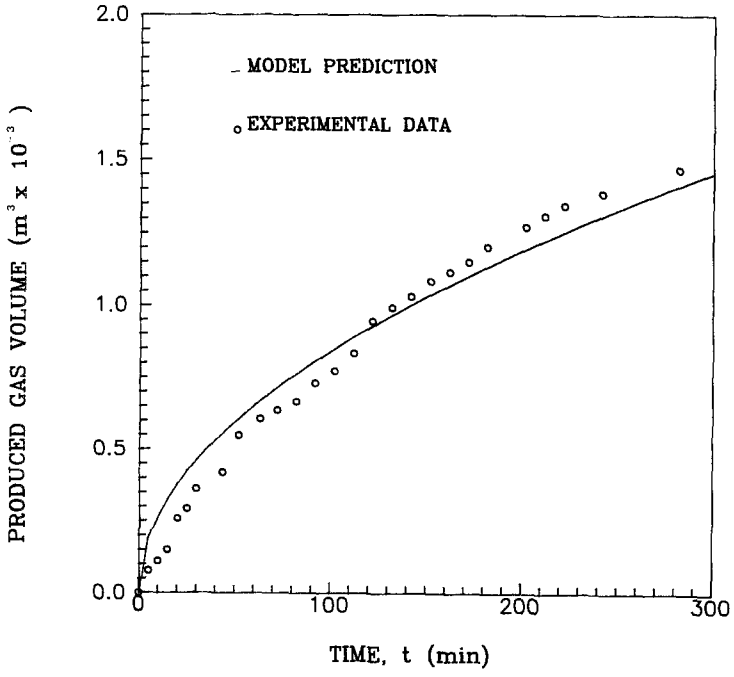

Fig. 13. Dissociated gas volume versus time for Run 3.

Figures 9 and 10 provide the volume of gas produced at 294 K and 90.94 KPa, as well as the position of the dissociation front, both as a function of time in Run 1. The moving boundary model results (solid line) discussed in the next section do not fit the data (circles) satisfactorily in either of these figures. On the other hand, Figures 11, 12, and 13 show that the data of Runs 2 and 3 are acceptably fitted by the moving boundary model, particularly during the period from 100 to 200 minutes. The reasons for the differences in response are discussed below, after a statement of the model equations and their solution.

4. Mathematical Model of Hydrate Dissociation

4.1. FORMULATION OF MODEL EQUATIONS

Consider a hydrate reserve in consolidated sediment at a uniform temperature slightly above the ice point, and at a uniform pressure P_i above that for three-phase (V–L_W–H) equilibria, P_D. The hydrate consists of pure methane for these initial estimations, and the entire system is maintained under isothermal conditions by an adequate flow of heat from the surrounding medium, assuming slow dissociation. The porous medium has a uniform porosity and occupies the semi-infinite region $0 < x < \infty$. Let S_H and S_g denote the uniform hydrate and gas saturations, respectively, so that εS_H is the volume fraction of the hydrate and εS_g is the volume fraction of the gas in the medium.

At time zero, the pressure at the boundary $x = 0$ is suddenly lowered to a constant value P_0 just less than the three-phase equilibrium value, P_D. The hydrate at the gas–hydrate interface will dissociate and there will be a moving dissociation interface at some distance $x = X(t)$ which separates the water–gas dissociated zone I from the hydrate–gas undissociated zone II. Thus, at any time $t > 0$, dissociated zone I occupies the region $0 < x < X(t)$ while the undissociated zone II occupies the region $X(t) < x < \infty$. Clearly, the following pressure distributions develop in the system: a pressure distribution $P_I(x, t)$ in region I with $P_0 < P_I(x, t) < P_D$ and a pressure distribution $P_{II}(x, t)$ in region II with $P_D < P_{II}(x, t) < P_i$.

In this model, dissociated water is assumed not to flow, but instead to contribute to the effective permeability of the system. The unidimensional continuity equation may be used to model the gas flow in the dissociated zone I as:

$$S_g \varepsilon \frac{\partial \rho}{\partial t} + \frac{\partial (\rho v)}{\partial x} = 0 \tag{2}$$

where the symbols are defined in the nomenclature section below. Darcy's Law may be used for the velocity v of the gas to obtain, for one dimension:

$$v = -\frac{\kappa}{\mu} \frac{\partial P}{\partial x}. \tag{3}$$

When Equation (3) is substituted into (2), along with the relationship for gas density ($\rho \equiv PM/zRT$), the following equation is obtained for constant viscosity and permeability:

$$\frac{1}{P}\frac{\partial P^2}{\partial t} = \frac{\kappa}{S_g \varepsilon \mu}\frac{\partial^2 P^2}{\partial x^2} \tag{4}$$

In Equation (4) the reciprocal pressure factor in the initial term causes the equation to be non-linear. If the pressure change in the system is restricted to a low value, the reciprocal of the average pressure P_{avg} ($\equiv [P_D + P_0]/2$) may be substituted as a constant in the first term of Equation (4) to remove the non-linearity.

For purposes of conforming to petroleum engineering nomenclature, we introduce the term for the correction of the gas volume in the pores, C_g:

$$C_g = \frac{1}{P} - \frac{1}{z}\left(\frac{\partial z}{\partial P}\right)_T. \tag{5}$$

The second term on the right is relatively minor under these conditions and may be assumed to be negligible, so that $C_{g_{avg}}$ may replace the first factor in Equation (4). Finally, the petroleum nomenclature change $C_t (\equiv S_g C_g)$ is used to obtain the equation for flow in the dissociated zone as:

$$\frac{\partial P_I^2}{\partial t} = \alpha_I \left(\frac{\partial^2 P_I^2}{\partial x^2}\right) \quad \text{for} \quad 0 < x < X(t),\ t > 0 \tag{6}$$

where:

$$\alpha_I \equiv \frac{\kappa_I}{\varepsilon C_{t_I} \mu_{g_I}} \tag{7}$$

and $X(t)$ is the position of the moving hydrate dissociation boundary. In the undissociated hydrate zone we can keep the same porosity ε by defining S_g as the fraction of the pore volume filled with gas. An equation similar to (6) is obtained for the undissociated phase:

$$\frac{\partial P_{II}^2}{\partial t} = \alpha_{II}\frac{\partial^2 P_{II}^2}{\partial x^2}, \qquad X(t) < x < \infty,\ t > 0 \tag{8}$$

where:

$$\alpha_{II} \equiv \frac{\kappa_{II}}{\varepsilon C_{t_{II}} \mu_{g_{II}}} \tag{9}$$

Equations (6) and (8) represent the primary equations for the pressure change with time in the dissociated and undissociated zones, respectively. Accompanying these two equations are four boundary conditions and two initial conditions. The initial conditions are:

$$P_{II} = P_i \quad \text{for} \quad 0 < x < \infty, \quad t = 0 \tag{10}$$

and

$$X(0) = 0 \quad \text{at} \quad t = 0 \tag{11}$$

The four boundary conditions are given in Equation (12)–(15):

$$P_I = P_0 \qquad \text{at} \quad x = 0, \qquad t > 0 \tag{12}$$

$$P_I = P_{II} = P_D \quad \text{at} \quad x = X(t), \quad t > 0 \tag{13}$$

$$P_{II} = P_i \quad \text{at } x = \infty, \quad t > 0 \tag{14}$$

and

$$\kappa_I \frac{\partial P_I^2}{\partial x} - \kappa_{II} \frac{\partial P_{II}^2}{\partial x} = \beta \frac{\partial x}{\partial t} \quad \text{at} \quad x = X(t), \quad t > 0 \tag{15a}$$

where:

$$\beta \equiv 2\varepsilon \mu_{g_D} P_D \left\{ S_H \omega_g \frac{\rho_H}{\rho_{g_D}} - (S_H - S_W) \right\}. \tag{15b}$$

All of the initial conditions and the boundary conditions are self-evident except (15), which requires a brief explanation. Equation (15) represents a jump gas mass balance at the dissociation interface [13]; it states that the change in mass flux across the moving hydrate interface is brought about by hydrate dissociation. The subscript D in equation (15b) indicates that the properties should be evaluated in the gas phase at the dissociation interface. The quantity ω_g in Equation (15b) represents the mass of the hydrocarbon gas contained in a unit mass of hydrate, which is given by:

$$\omega_g = \frac{M_g}{n_H M_W + M_g} \tag{15c}$$

where n_H is the hydrate number. Using a statistical thermodynamics model [15] we estimated the occupancy of the cages at 93.5% for n_H of 6.15 at our experimental conditions. The quantity S_w in Equation (15b) represents the water saturation in the dissociated zone I, which is easily found as:

$$S_W = \frac{V_{g_W}}{V_{g_W} + V_{g_F} + V_{g_D}} \tag{15d}$$

where:

$$V_{g_W} = \varepsilon S_H (1 - \omega_g) \rho_h / \rho_W,$$

$$V_{g_F} = \varepsilon (1 - S_H)$$

and

$$V_{g_D} = \varepsilon S_H \omega_g \rho_H / \rho_{g_D}.$$

In the above equations, V_{g_F} represents the volume fraction of the free gas prior to dissociation; V_{g_D} and V_{g_W} represent the volume fraction of the gas and water released during dissociation, respectively.

4.2. SOLUTIONS TO MODEL EQUATIONS

The analytical solution to the boundary-value problem given by Equations (6) through (15) is similar to the Neumann problem of heat conduction during melting or solidification of a semi-infinite region [3]. The solution yields the pressure profiles within each zone, as:

$$\frac{P_{\mathrm{I}}^2 - P_0^2}{P_{\mathrm{D}}^2 - P_0^2} = \frac{\operatorname{erf}(a\eta)}{\operatorname{erf}(a\xi)}, \tag{16}$$

$$\frac{P_{\mathrm{II}}^2 - P_i^2}{P_{\mathrm{D}}^2 - P_i^2} = \frac{\operatorname{erfc}\eta}{\operatorname{erfc}\xi}. \tag{17}$$

In Equations (16) and (17) the following dimensionless groups were used:

$$a = \left(\frac{\alpha_{\mathrm{II}}}{\alpha_{\mathrm{I}}}\right)^{1/2}; \tag{18}$$

$$\eta = \frac{x}{\sqrt{4\alpha_{\mathrm{II}} t}}; \tag{19}$$

and

$$\xi = \frac{X(t)}{\sqrt{4\alpha_{\mathrm{II}} t}}. \tag{20}$$

It may be shown that the value of ξ in Equation (20) is a constant which relates the position of the moving boundary $X(t)$ to the square root of time t. The value of ξ is obtained through the differentiation of Equations (16) and (17) for use in the final boundary Equation (15). As a result, a transcendental equation is obtained for ξ, as:

$$a\left[\frac{\chi_{\mathrm{I}}(P_{\mathrm{D}}^2 - P_0^2)}{\chi_{\mathrm{II}}(P_i^2 - P_{\mathrm{D}}^2)}\right]\frac{\exp(-a^2\xi^2)}{\operatorname{erf} a\xi} - \frac{\exp(-\xi^2)}{\operatorname{erfc}\xi} = \frac{\sqrt{\pi}\,\alpha_{\mathrm{II}}\beta}{\chi_{\mathrm{II}}(P_i^2 - P_{\mathrm{D}}^2)}\xi. \tag{21}$$

When the iterative solution of Equation (21) for ξ is obtained, that value may be substituted back into Equations (16), (17), and (20) to obtain the pressure profiles and the position of the moving hydrate boundary $X(t)$ with time. The position of the moving boundary with time may be compared with the experimental values for the time of increase of the resistances along the core length. The volume of gas produced from the core may also be obtained for comparison with experiment from the value of ξ via the equation:

$$\frac{Q}{A_{\mathrm{c}}} = \frac{a\chi_{\mathrm{I}}}{\mu_{\mathrm{I}} P_0 \sqrt{\pi a_{\mathrm{II}}}} \frac{P_{\mathrm{D}}^2 - P_0^2}{\operatorname{erf} a\xi}\sqrt{t}. \tag{22}$$

The above solution is applicable to semi-infinite media. In a typical experiment however, a core of finite length L is used and the solution obtained is not strictly applicable. Modification of the solution to allow for a finite medium of length L requires replacement of the outer boundary condition (Equation 14) by the condition of zero flux ($\partial P_{\mathrm{II}}/\partial x = 0$ at $x = L$). Under this circumstance the boundary-value problem does not admit an analytical solution and one must resort to a numerical solution. However, for short times the semi-infinite solution presented here is still applicable.

Figures 9 through 13 contain predictions (solid lines) from Equations (21) and (22) for the gas produced and the position of the moving boundary for Runs 1, 2 and 3. Table I contains the values of the parameters used in the above equations.

Table I. Parameters for use in hydrate depressurization model

Parameter/Run	1	2	3
P_0, Pa	1 468 635	2 502 885	2 642 164
P_i, Pa	3 970 141	3 173 079	4 250 078
χ_I, m^2	3×10^{-17}	5×10^{-17}	6×10^{-18}
χ_{II}	2×10^{-18}	1.31×1^{-17}	3×10^{-18}
ε	0.188	0.188	0.1978
S_W	0.375	0.55	0.537
χ_{abs}, m^2	9.869×10^{-14}	9.869×10^{-14}	8.388×10^{-14}
ξ	0.84099	0.0928	0.17524
α_{II}, m^2/s	5.908×10^{-6}	5.055×10^{-5}	1.3188×10^{-5}
Produced Water	16.8%	40%	25.2%

5. Discussion of Experimental and Predicted Results

The data of Run 1 were not predicted well by the model, as is shown particularly in Figure 9, for the volume of gas produced as a function of time. For Run 1, Figure 3 shows that the inlet pressure decreased to a lower value than the outlet pressure, indicating that most of the hydrates formed a plug near the beginning of the core, with a smaller amount near the outlet. The gas volume versus time curve of Figure 9 shows an initial linear production rate such as might come from the compressed gas which occupies the outlet of the core. The linear production period is followed by a period during which the volume varies with the square root of time, as might occur when the hydrate at the beginning of the cores dissociates. In any case, for Run 1, the outlet pressure during dissociation was approximately one-half of the equilibrium pressure, so that the model assumption of an average pressure may not be strictly applicable.

The data of Run 2 were satisfactorily approximated by the model equations. Figure 4 does not show a crossover of the inlet and outlet pressures on hydrate formation, but instead indicate a more uniform formation throughout the core with time. Figures 11 and 12 show that the very early time data do not agree well with the model, perhaps due to either a free compressed gas release, or a large amount of water produced early on. At later times the volumetric output and the front movement both showed good agreement with the results of the model for Run 2.

Figure 13 shows good agreement between the model and the experimental results. As indicated earlier, the inlet and outlet pressures were equilibrated through two cycles of the annealing process resulting in better hydrate distribution along the core. We would expect the model to represent the data better for this case in which the hydrate is uniformly distributed across the porous media, with only an incremental pressure drop.

6. Future Experimental and Modeling Research

We anticipate continuing the experimental work, with other temperatures and cores. In the model development, the next step will be to develop a numerical solution for

the finite medium. Predictions from the analytical model can then be compared to the numerical solution for all time.

Acknowledgements

This work was sponsored by the United States Department of Energy (U.S.D.O.E.) under contract DE-FG21-86MC23063. The East-China Petroleum Institute and the Ministry of Petroleum Industry of the Peoples Republic of China are gratefully acknowledged for the sponsorship of Professor Li as a Visiting Scholar in this laboratory. Dr. W. F. Lawson of the U.S.D.O.E. Morgantown Energy Technology Center kindly loaned us the injection pump, pressure controller, and the core holder.

Appendix: Nomenclature

A_c = cross-sectional area of the core, m^2;
a = constant in Equation (18);
C_g = gas compressibility, 1/Pa;
C_t = total compressibility, 1/Pa;
erf = error function;
erfc = complementary error function;
M = gas molecular mass, kg/kg-mol;
P_i = initial gas pressure, Pa;
P_0 = gas pressure at $x = 0$, Pa;
P_D = dissociation pressure, Pa;
Q = volumetric flow rate, m^3/s;
R = universal gas constant, J/kg mol K;
S_g = gas saturation, dimensionless;
S_H = hydrate saturation, dimensionless;
S_W = water saturation, dimensionless;
T = temperature, K;
t = time, s;
v = superficial gas velocity, m/s;
V_{g_D} = volume fraction of dissociated gas, dimensionless;
V_{g_F} = volume fraction of free gas prior to dissociation, dimensionless;
V_{g_W} = volume fraction of dissociated water, dimensionless;
$X(t)$ = position of dissociation front, m;
x = axial position, m;
z = compressibility factor, dimensionless;

α = constant, Equation (7), m^2/s;
ε = porosity, dimensionless;
η = similarity variable ($\equiv x/(4\alpha_{II}t)^{1/2}$), dimensionless;
χ = permeability, m^2;
μ = gas viscosity, Pa·s;
ξ = constant, Equation (20), dimensionless;
ρ = density, kg/m^3;

ρ_g = gas density, kg/m^3;
ρ_H = hydrate density, kg/m^3;
ρ_W = water density, kg/m^3;
ω_g = mass of gas produced per unit mass of hydrate, dimensionless;

SUBSCRIPTS

I = dissociated zone I;
II = hydrate zone II;
D = dissociation;
g = gas;
H = hydrate;
i = initial condition;
0 = boundary condition at $x = 0$;
W = water.

References

1. P. E. Baker: in *Natural Gases in Marine Sediments*, Ed. I. R. Kaplan, Plenum, 1974, p. 227.
2. G. A. Bayles, W. K. Sawyer, H. R. Anada, S. Reddy, and R. D. Malone: *Chem. Eng. Commun.* **47**, 225 (1986).
3. H. S. Carslaw and J. C. Jaeger: *Conduction of Heat in Solids*, Clarendon Press, Oxford, 1959.
4. N. V. Cherskii and Y. Makogon: *Oil Gas Invest.* **10**, 82 (1970).
5. N. V. Cherskii and E. A. Pondarev: *Dokl. Akad. Nauk. SSSR.* **203**, 550 (1972).
6. D. W. Davidson: *Clathrate Hydrates*, (*Water – A Comprehensive Treatise* vol. 2, Ed. F. Franks) Plenum, 1973, p. 115.
7. D. W. Davidson, M. K. El-Defrawry, M. O. Fuglem, and A. S. Judge: *Int. Conf. Permafrost Proc.* **3**, 937 (1978).
8. A. I. Evrenos, J. Heathman, and J. Ralston: *J. Petrol Tech.* **23**, 1059 (1971).
9. G. D. Holder, P. F. Angert, V. T. John, and S. Yen: *J. Petrol. Tech.* **34**, 1127 (1982).
10. V. A. Kamath, G. D. Holder, and P. F. Angert: *Chem. Eng. Sci.* **39**, 1435 (1984).
11. K. A. Kvenvolden and M. A. McMenamin: *U.S. Geol. Surv. Circ.* **825** (1980).
12. Y. F. Makogon: *La Recherche* **18**, 1192 (1987).
13. J. C. Slattery: *Momentum, Heat, and Mass Transfer in Continua*, R. E. Krieger Co., Melbourne, FL, 1978.
14. J. W. Ullerich, M. S. Selim, and E. D. Sloan: *AIChE J.* **33**, 747 (1987).
15. J. H. van der Waals and J. C. Platteeuw: *Clathrate Solutions* (Adv. Chem. Phys. vol. 2 Ed. I. Prigogine), Interscience, 1959, pp. 1–58.
16. J. S. Weaver and J. M. Stewart: *Fourth Can. Permafrost Conf. Proc.* 312 (1982).